The Monte Carlo Method: Versatility Unbounded In A Dynamic Computing World
Chattanooga, Tennessee, April 17–21, 2005, on CD-ROM, American Nuclear Society, LaGrange Park, IL (2005)

A DIRECTIONAL SPECTRUM MODEL FOR A 6 MV PHOTON BEAM FROM AN ELEKTA SLI MEDICAL LINEAR ACCELERATOR

Andy Ma
Centre for Nuclear and Radiation Physics
Department of Physics, University of Surrey
Guildford, Surrey, GU2 7XH, United Kingdom
a.ma@surrey.ac.uk

Sultan Khalil
Radiotherapy Physics Department
Poole General Hospital NHS Trust
Longfleet Road, Poole, Dorset, BH15 2JB, United Kingdom
sultan.khalil@poole.nhs.uk

Josef Dubicki and Nicholas M. Spyrou
Centre for Nuclear and Radiation Physics
Department of Physics, University of Surrey
Guildford, Surrey, GU2 7XH, United Kingdom
jdubicki@koc.mtw-tr.nhs.uk; n.spyrou@surrey.ac.uk

ABSTRACT

In the simulation of a 6MV photon beam from an Elekta SLi medical linear accelerator, a phase space file recording all the particles crossing a surface downstream of the monitor chamber was created. Since a phase space file is large and inconvenient to manipulate, various authors have developed models to describe the data in a compact format, for example, the single source model, the multiple source model and the correlated histogram model. The particle energy and flight direction in these models are loosely related. In our directional spectrum approach of modelling the data, the energy sampling was coupled to its flight direction. As the beam emerging from the monitor chamber is symmetrical around the central axis, the particle location can be expressed by its radial distance from the central axis and its flight direction in terms of its deviation from the imaginary fan-line joining its position on the phase space plane to the electron target. Comparisons of the dose distributions calculated by our model with measurements showed that the difference was generally within 2%. Thus, our new approach of phase space modelling is capable of representing the original phase space data accurately and compactly. Furthermore, it is suitable for predicting dose distributions in a variety of field sizes.

Key Words: Monte Carlo, medical linac, phase space modelling

1 INTRODUCTION

The Monte Carlo method is generally accepted as the most accurate method in predicting the radiation field generated by a medical linear accelerator (linac), and quantities arising from this field [1], [2], [3]. It can provide valuable data that is difficult or impractical to measure [4]. However, the Monte Carlo simulation of the treatment head of a linac can be very time consuming. It is common practice to break the simulation into two or more steps such that the

results from one step become the input to the next (Figure 1). Once the simulation of the patient-independent parts (from the electron target to the end of the ionisation chamber) is completed, the results can be used for further simulations downstream with different collimator settings, or even further interaction of the radiation field inside different patients. Significant simulation time can thus be saved from this simple procedure.

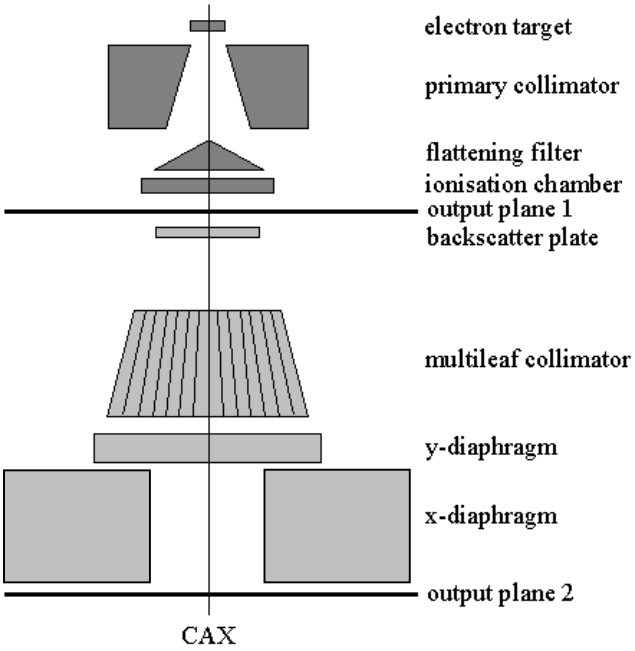

Figure 1. Schematic diagram of an Elekta SLi linac. Output plane 1 is where our directional spectrum model applied. Output plane 2 is used for further simulations downstream.

The result of the simulation from the patient-independent parts is the information of all the particles emerging from the ionisation chamber before their further interactions with other components in the treatment head. This collection of particle information is a phase space. The more particles that are simulated, the less statistical fluctuation in further simulations. Therefore, the information of a large number of particles is recorded in a phase space file. A full phase space file is typically in gigabytes which is inconvenient to manipulate.

Several models have been developed to describe the phase space information. The information extracted from the full phase space file under these models only requires kilobytes of storage space. An additional advantage of using phase space modelling is that the statistics in future simulations is no longer dictated by the number of particles in the full phase space file. The models, theoretically, allow the generation of unlimited number of particles.

One way to model the phase space is to tally the particle fluence and energy spectrum at different radial distances from the central axis (CAX). In the reconstruction of the phase space, the particles are sampled according to the fluence distribution and the corresponding spectrum and their flight directions are assumed to be focused at the electron target [5]. With an electron sub-source and Gaussian blurring of the beam penumbra, it was found [5] that this model was

within the criteria set out by the Radiation Therapy Committee of the American Association of Physicists in Medicine [6].

Liu et al [7] considered a dual source approach in which an extra-focal source was incorporated into a focused primary source. An electron sub-source was also included in their model.

The correlated histogram approach was put forward by Schach von Wittenau et al [8]. They characterised the photons generated in each head component and a series of histograms were constructed to depict the probabilities of particles from each head component reaching the isocentric plane through the output plane. Sampling these histograms gave the particle's flight direction, energy and weight. Then, the particle was backtracked to the base of the ionisation chamber and transported downstream. This model was subsequently incorporated into the Monte Carlo dose calculation system, PEREGRINE, and it was shown that the calculations agreed very well with the measurements [9].

Deng et al [10] suggested the use of multiple source model in which particles were sampled from three sub-sources representing the electron target, the primary collimator and the flattening filter. Fix et al [11] devised a similar model with twelve sub-sources. Particles were backtracked to the surface of a component in the treatment head. A distribution of particle origin was obtained and plane sources were constructed for each head component. In the reconstruction of the phase space, particles were sampled on the output plane according to the fluence distribution of the plane. The flight direction of a particle was determined by the line joining its starting position on the output plane and its position on the source plane, which was obtained from the distribution of particle origin and the fluence distribution in the source plane. Particle energy was sampled according to the corresponding source plane. Comparison between the multiple source model calculations and full phase space calculations showed agreements within 1% in fields up to $15\times15\text{cm}^2$.

Models accounting for both the fluence and the spectral variations performed the best. Models disregarding either one of the variations did not measure up to those disregarding both, because a constant fluence and a constant spectrum is a good approximation to the radiation field [3]. The correlated histogram model and the multiple source model also preserved the particle's flight direction to a large extent.

Ma and Spyrou [12] attempted to model the particle's flight direction explicitly with their directional spectrum model. The particle energy is coupled tightly to its flight direction. The objective of this study was to compare this model with measurements.

2 THE DIRECTIONAL SPECTRUM MODEL

Symmetry around the CAX was generally assumed for the phase space data below the ionisation chamber (output plane 1 in Figure 1) [5] [7] [13]. Siebers et al [13] also suggested a compression technique for the phase space file by taking advantage of the symmetry. All particles at (x,y,z) with direction cosines (u,v,w) were rotated onto the x-axis (Figure 2) with the following equations (1).

$$
\begin{aligned}
x' &= r = \sqrt{x^2 + y^2} \\
y' &= 0 \\
z' &= z \\
u' &= (ux + vy)/r \\
v' &= (vx - uy)/r \\
w' &= w
\end{aligned}
\tag{1}
$$

Since z was a constant for all particles on the output plane, the particle position could be represented by r alone. For w', only its sign was necessary for storage; its magnitude could be obtained from the identity equation (2).

$$
u'^2 + v'^2 + w'^2 = 1 \tag{2}
$$

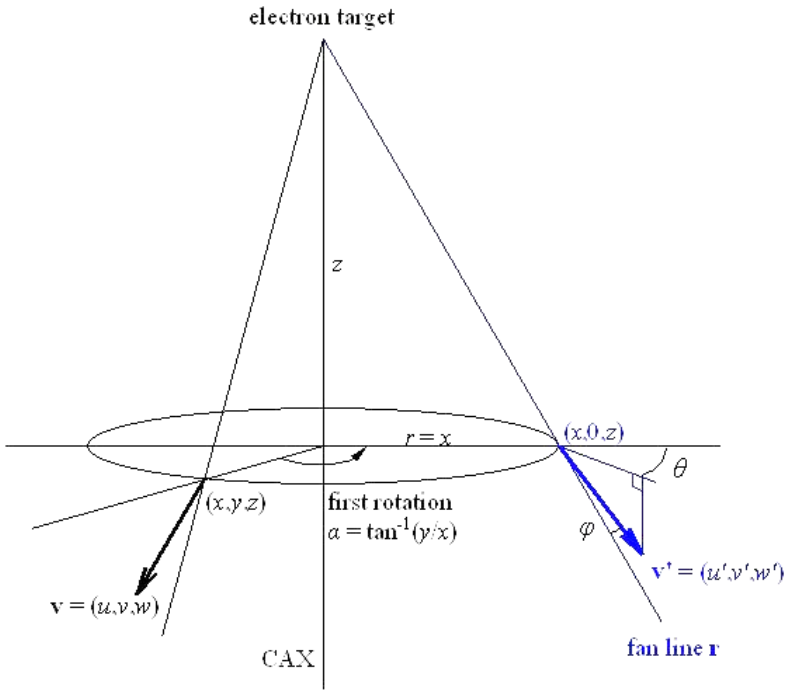

Figure 2. The directional spectrum model. The particles are compressed onto the x-axis and the energy specrtrum is associated with the radial position *r* and the normalized scattering angle *φ*. The azimuthal angle *θ* has no importance in the model.

Very importantly, the relative particle flight directions were preserved under the rotation. Compressing the particles of the same annular ring onto a point also enabled the characterisation of the directional distribution of the particles. In particular, we examined the deviation of the flight paths from the fan line joining the electron target and the annular ring. This deviation or

normalized scattering angle φ can be defined by the dot product of the flight direction $\mathbf{v}'$ and the fan line **r (**Figure 2**)**:

$$\cos\varphi = \frac{\mathbf{r}\cdot\mathbf{v}'}{|\mathbf{r}||\mathbf{v}'|} \tag{3}$$

Furthermore, the normalized azimuthal angle θ of the vector $\mathbf{v}'$ around **r** has been shown to have negligible effect in the model [12]. Thus the spectrum is a function of photon energy, the normalized azimuthal angle and the radial position from the central axis:

$$\frac{\mathrm{d}}{\mathrm{d}E}\Phi'(E,\varphi,r) = \int_{\theta}\left[\frac{\mathrm{d}}{\mathrm{d}E}\Phi(E,\varphi,\theta,r)\right]\mathrm{d}\theta \tag{4}$$

3 MATERIALS AND METHODS

3.1 Modelling the Elekta SLi treatment head

MCNPX version 2.4.0 [15] was used for the simulations. Its photon transport, essentially the same as MCNP4C2 [16], has two modes – simple physics treatment and detailed physics treatment. The simple physics treatment includes photoelectric effect without fluorescence, Compton scattering on free electrons and pair production. The detailed physics treatment accounts for the fluorescence after photoelectric absorption and the electron binding effects with form factors. Rayleigh scattering is also included in the detailed physics treatment. The electron transport employs the condensed history technique in which the electron path is broken down into major steps and the energy loss and straggling are pre-calculated for each step according to the Landau theory [17]. Within each major step, the path is further divided into m sub-steps where m depends on the medium. The angular deflection of the electron trajectory is sampled at the end of each sub-step according to the Goudsmit-Saunderson theory [18]. Secondary particles including knock-on electrons, K- and L-shell fluorescence and bremsstrahlung photons are produced during each sub-step.

The modelled head components included the electron target, the primary collimator, the 6MV flattening filter, the ionisation chamber, the backscatter plate, the multileaf collimator (MLC), the y-diaphragms and the x-diaphragms (Figure 1). The MLC consisted of 80 independent, doubly focused leaves in two opposite banks. Each leaf had a width of 11 mm and a pitch of 10 mm projected at the isocentre due to its stepped edges [14]. All leaves were modelled individually with air gaps in-between. The x- and y-diaphragms were back-up collimators moving in orthogonal directions. The parameters of the initial electron beam (the beam incidence on the electron target) were obtained by matching the calculated percentage depth dose (PDD) curve to the measured PDD. The beam had a mean energy of 6.5 MeV with full width half maximum (fwhm) 1 MeV. Furthermore, it was assumed to be a uniform parallel beam of 1 mm in diameter. Other transport parameters included detailed physics treatment and low energy cut-

off at 10 keV for photon transport, and ITS-style energy indexing and low energy cut-off at 189 keV for electron transport.

In our previous study [12], all particles emerging from the ionisation chamber were written to an MCNPX surface source file. An IDL programme was developed in-house to extract the phase space data from the surface source file. In this study, we wrote the *tallyx* subroutine to obtain the directional spectrum at output plane 1. The *tallyx* subroutine worked in conjunction with

1. a type 1 surface current tally,

2. a tally segment (*FSn*) card that set up the radial bins, a tallyx input (*FUn*) card that set up the cosine bins and

3. a tally energy (*En*) card that set up the energy bins.

The type 1 surface current tally by itself gives the total number of particles crossing a plane. The *FSn* and the *En* cards divide the tally into bins in the usual MCNP/MCNPX manner. The *FUn* card was chosen over the usual tally cosine (*Cn*) card because the *Cn* card works with a single reference vector but our reference vector (the fan line) depends on the particle position. Thus, our *tallyx* subroutine examines the particle's radial position on the output plane, its energy and its direction of crossing with respect to the fan line. The appropriate bin of the tally will then be credited with a particle.

3.2 Beam rescontruction

The distributions generated under our model included:

1. a radial fluence distribution describing the number of particles in the 25 rings or radial bins (0 cm $\leq r \leq$ 5cm, 0.2 cm bin size),

2. twenty five angular fluence distributions ($0° \leq \varphi \leq 45°$, 0.1° bin size at small and variable bin sizes at larger , 13 bins in total) associated with each of the 25 radial bins, describing the number of particles per unit scattering angle with respect to the fan lines and

3. three hundred and twenty five energy spectra (0 MeV $\leq E \leq$ 7 MeV, 0.2 MeV bin size) for each combination of the 25 radial bins and 13 scattering angle bins.

All distributions were translated into the MCNP/MCNPX *SIn* and *SPn* card format and incorporated into the simulation input file. When the *SDEF* source definition is not present in the input file, MCNPX will rely on the *source* subroutine to generate the particles. It is also possible to pass some control parameters from the input file into *source* through the *IDUM* and the *RDUM* cards. These parameters include the numbers of distributions in the above list, the position of the phase space plane and the Gaussian source biasing details as described below. An electron sub-source was also included.

The *source* subroutine is essentially the reverse process of the *tallyx* subroutine. A particle is first sampled for its radial position which will subsequently be converted into Cartesian coordinates with the assumption of symmetry around the CAX. The appropriate angular fluence distribution is then sampled for the flight direction. Finally, the energy spectrum corresponding to the particle's radial position and its flight direction is sampled for the particle energy.

To increase the computation efficiency, we had written into the *source* subroutine a variance reduction technique of Gaussian source position biasing. The radial fluence probability distribution is multiplied by a Gaussian probability density function with a mean equal to the radial position of the field centre and a full width half maximum equal to eight times the field size back-projected onto the phase space plane. The particle weight was adjusted by the inverse of the Gaussian probability density function. The factor eight was chosen so that the Gaussian function would not decrease to zero too rapidly and the radial position sampling was not over-biased.

The generated beam was transported from output plane 1 through the beam modifiers to the second output plane beneath the treatment head. It was then transported into a water tank at 100 cm SSD. The percentage depth dose curves were calculated at 5 mm intervals up to 30 cm deep with voxel size $2\times2\times5$ mm^3. The lateral dose profiles were calculated at 5 mm grids at two depths – 1.5 cm and 10 cm – with voxel size $5\times5\times5$ mm^3. Type 3 energy deposition mesh tallies were used, i.e., kerma approximation of the dose was implicit in the calculations. The particles on the second output plane were reused several times [13] to improve the statistics.

3.3 Measurements

The beam profiles and depth ionization curves were all generated using the Scanditronix Wellhofer water tank scanning system (Wellhofer, Germany) which consists of a $48\times48\times48$ cm^3 water tank and a three-dimensional (3D) scanning mechanism. The manufacturer's specification of repeatability of positioning the chambers with the scanning system is ±2 mm. The SLi linac was setup with gantry angle at 0º and diaphragm angle at 90º. The MCU movement controller was connected to a laptop computer with the Scanditronix Wellhofer OmniPro-Accept software for data collection. The positioning of the water tank was done by setting the tank x-axis to correspond to the linac x-size. Together with the 90º diaphragm angle, this geometry gave crossline scans in the AB direction and inline scans in the GT direction. The centre of the tank coincided with the linac central axis and with the centre of the scanning area in a horizontal plane for the central axis PDD and symmetrical profiles. Vertical height adjusted for the required focus-to-axis distance (FAD) of the scans. Scanning movements along x and y coordinates coincide with the crosswires. This was checked by moving the ion chamber along each of x and y coordinates to the limits.

The tank was filled with water for minimum depth appropriate for measurements – 10 cm below the greatest PDD measurement depth. A minimum 10 cm water margin between the nominal field size and the scanning area were also observed. The tank level was checked with a circular black levelling disc.

The ion chamber used for the scanning was an RK ion chamber, with an active volume of 0.12 cm^3 and an inner cavity radius is 2.0 mm. The chamber position was corrected for effective point of measurement for 6 MV – it was moved 1 mm away from x-ray source. After the chamber had been positioned at the effective point of measurement, the scanning origin was set at this point. Depths (z coordinates) represented the actual measurement depths. A reference detector was positioned at the corner of the field using a holder. High voltage (HV) for chamber was -200V.

4 RESULTS AND DISCUSSIONS

Three fields were simulated as described in section 3.2 and compared with measurements: 5×5 cm^2, 10×10 cm^2 and 20×20 cm^2 on axis. Each set of comparisons consists of a percentage depth dose curve and two lateral dose profiles at 1.5 cm deep (d_{max}) and at 10 cm deep. All data were normalized to 1 on CAX at 1.5 cm deep. They are shown in Figure 3.The simulations were continued until all relative errors were below 10%. Within the field, the relative errors in the lateral profiles were between 0.5% and 2%. The large relative errors (near 10%) occurred outside the field because there were less particles. For the PDD curves, all relative errors were less than 0.1%.

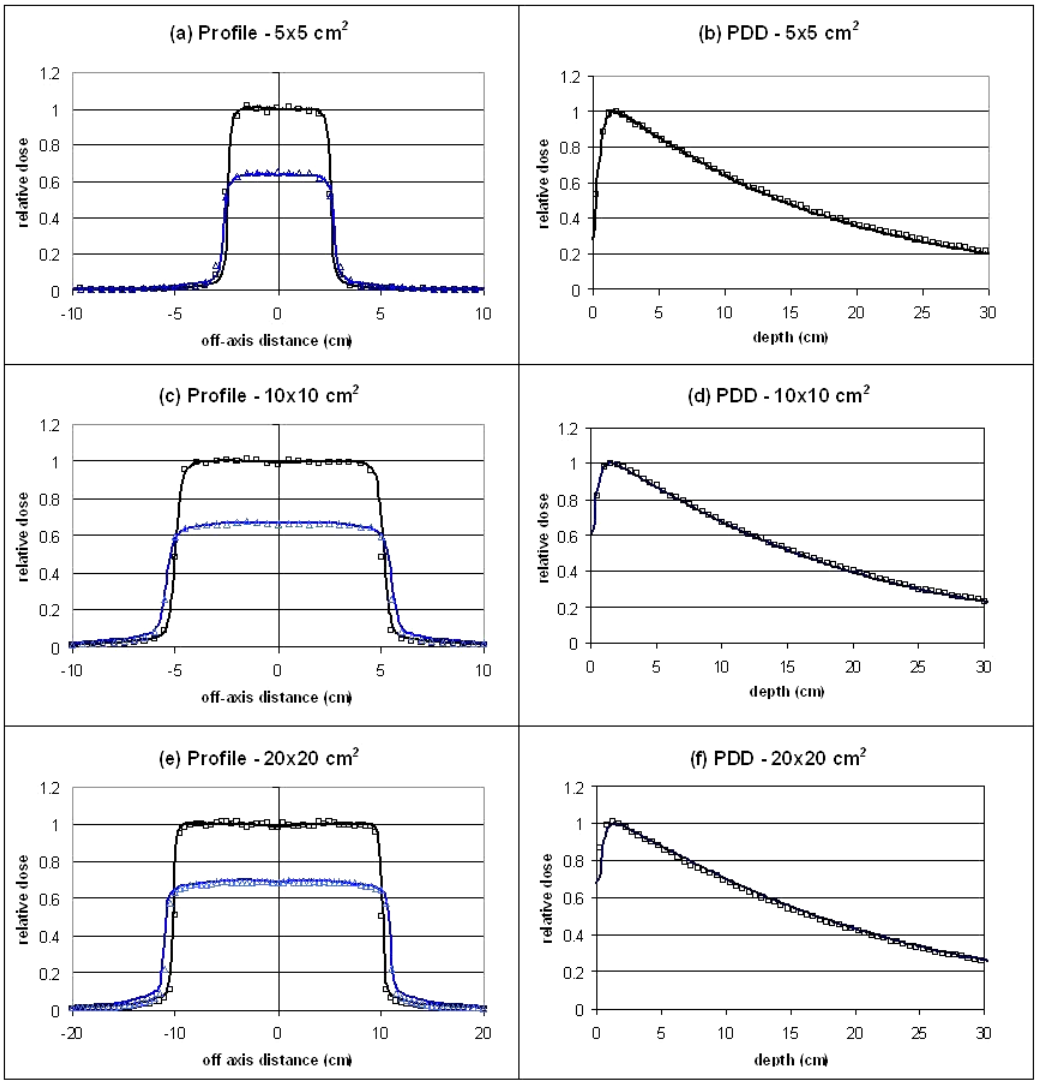

Figure 3. Calculated and measured dose curves. The profiles are at 1.5 cm deep (black) and 10 cm deep (blue). In all graphs, the solid lines represent the measurements while the squares and the triangles are calculated with the directional spectrum model. The error bars are not shown for clarity. All relative errors are below 10%.

When compared to the measurements, the differences between calculated and measured beam profiles and PDD were generally less than 2% of the maximum dose at the small dose gradient regions – within and outside the field. In the large dose gradient regions – the penumbra, the shifts were within 2 mm.

According to the manufacturer, the initial electron beam has a full width half maximum of 1 mm. It was assumed to be a uniform beam of 1 mm in diameter when we obtained our phase space data. This approximation may have some effect on the virtual spot size of the bremsstrahlung beam. Our results have shown that this approximation does not have any significant effect on the dose distribution in the water phantom for 5×5 up to 20×20 cm^2 fields. However, the change of spot size may have some effect on very small fields (e.g. 1×1 cm^2) although we expect this effect will be small. It warrants further investigations.

5 CONCLUSIONS

We have presented a new phase space modeling technique that we termed the directional spectrum model. Very good agreements, in terms of lateral dose profiles and percentage depth dose curves, have been obtained in the comparisons with physical measurements from 5×5 cm^2 field to 20×20 cm^2 fields. The agreements are better than 2% in general and the shift in the isodose curve is less than 2 mm. This means that the model represents the original phase space data accurately and compactly. Furthermore, the model directly couples the energy spectrum to the position and flight direction of the particles. This is a novel technique for examining the phase space data. Further studies of its performance in very small fields (e.g. 1×1 cm^2) and large fields (e.g. 40×40 cm^2) shall be carried out.

6 REFERENCES

1. R. Mohan, "Why Monte Carlo?" *Proceedings of the XIIth International Conference on the Use of Computers in Radiation Therapy*, Salt Lake City, USA, 27–30 May 1997, pp.16–18 (1997)
2. P. Andreo, D. T. Burns, K. Hohlfeld, M. S. Huq, T. Kanai, F. Laitano, V. G. Smyth and S. Vynckier, *Absorbed Dose Determination in External Beam Radiotherapy: An International Code of Practice for Dosimetry Based on Standards of Absorbed Dose to Water IAEA TRS-398*, International Atomic Energy Agency, Vienna, Austria 2001
3. F. Verhaegen and J. Seuntjens, "Monte Carlo modelling of external radiotherapy photon beams," *Phys. Med. Biol.* **48** R107–R164 (2003)
4. P. Andreo, "Monte Carlo techniques in medical radiation physics," *Phys. Med. Biol.* **36** pp.R861–R920 (1991)
5. I. Chetty, J. J. DeMarco and T. D. and T. D. Solberg, "A virtual source model for Monte Carlo modelling of arbitrary intensity distributions," *Med. Phys.* **27** pp.166–172 (2000)
6. B. Fraass, K. Doppke, M. Hunt, G. Kutcher, G. Starkschall, R. Stern and J. Van Dyke, "American Association of Physicists in Medicine Radiation Therapy Committee Task Group 53: Quality assurance for clinical radiotherapy treatment planning," *Med. Phys.* **25** pp.1773–1829 (1998)

7. H. H. Liu, T. R. Mackie and E. C. McCullough, "A dual source photon beam model used in convolution/superposition dose calculations for clinical megavoltage x-ray beams," *Med. Phys.* **12** pp.1960–1974 (1997)

8. A. E. Schach von Wittenau, L. J. Cox, P. M. Bergstrom, W. P. Chandler and R. Mohan, "Correlated histogram representation of Monte Carlo derived medical accelerator photon-output phase space," *Med. Phys.* **26** pp.1196–1211 (1999)

9. C. L. Hartmann Siantar, R. S. Walling, T. P. Daly, B. Faddegon, N. Albright, P. Bergstrom, A. F. Bielajew, C. Chuang, D. Garrett, R. K. House, D. Knapp, D. J. Wieczorek and L. J. Verhey, "Description and dosimetric verification of the PEREGRINE Monte Carlo dose calculation system for photon beams incident on a water phantom," *Med. Phys.* **28** pp.1322–1337 (2001)

10. J. Deng, S. B. Jiang, A. Kapur, J. Li, T. Pawlicki and C-M Ma, "Photon beam characterization and modelling for Monte Carlo treatment planning," *Phys. Med. Biol.* **45** pp.411–427 (2000)

11. M. K. Fix, M. Stampanoni, P. Manser, E, J. Born, R. Mini and P. Rüegsegger, "A multiple source model for 6 MV photon beam dose calculations using Monte Carlo," *Phys. Med Biol.* **46** pp.1407–1427 (2001)

12. A. Ma and N. M. Spyrou, "A new single source model of a 6 MV photon beam," *Abstracts of the Advanced Workshop on Current Topics in Monte Carlo Treatment Planning*, Montreal, Canada, 3–5 May 2004, pp.77 (2004)

13. J.V. Siebers, P. J. Keall, B. Libby, R. Mohan, "Comparison of EGS4 and MCNP4b Monte Carlo codes for generation of photon phase space distributions for a Varian 2100C," *Phys. Med. Biol.* **44** 3009–26 (1999)

14. A. R. Hounsell and T. J. Jordan, "Quality control aspects of the Philips multileaf collimator," *Radioth. and Oncol.* **45** pp.225–233 (1997)

15. Waters L S (ed) *MCNPX User's Manual, Version 2.4.0 LA-CP-02-408*, Los Alamos National Laboratory, Los Alamos, USA (2002)

16. J. F. Briesmeister (ed) *MCNP – A General Monte Carlo N-Particle Transport Code, Version 4C, LA-13709-M*, Los Alamos National Laboratory, Los Alamos, USA (2000)

17. L. Landau, "On the energy loss of fast particles by ionization," *J. Phys. USSR* **8** pp.201–205 (1944)

18. S. Goudsmit and J. L. Saunderson, "Multiple scattering of electrons," *Phys. Rev.* **57** pp.24–29 (1940)